RESEARCH ARTICLE

Heat Transfer and Thermal Radiation Inspection of MHD Flow of Hybrid Nanofluid with Variable Viscosity and Thermal Conductivity Using Various Shapes

Bharat Kumar[1] and **Ravi Gupta**[2,*]

[1] Multanmal Bhickhchand Chhajer, Government Girls College, Barmer 344001, India
[2] School of Science and Technology, Vardhman Mahaveer Open University, Kota 324010, India

Abstract

This paper explores heat transfer and MHD flow of different shapes of (Ag-TiO_2/PAO Oil) hybrid nanoparticles through an unsteady radially stretching sheet consider variable thermal conductivity and viscosity. The present investigation explores the thermal radiation impact of different shapes (platelet, sphere, brick, blade, cylinder) of hybrid nanoparticles with variable viscosity(μ_{hnf}) and thermal conductivity(k_{hnf}) under the suction and partial slip parameter. This study presents a novel analysis of variable thermal conductivity and viscosity for different shapes of hybrid nanoparticles. The nonlinear ODEs are generated by proper transformation from governing partial differential equations. A numerical technique (BVP4C) is used to solve nonlinear ODEs in MATLAB. Supported by numerous graphs and tables, we discussed the impact in velocity and temperature profile influence by different physical parameters, and also Nusselt number, skin friction coefficient are investigated. An increase in variable viscosity and thermal conductivity parameters causes velocity profile decreases. Platelet-shaped nanoparticles have higher velocity and heat transfer rate compared to nanoparticles of other shapes. We have observed that velocity profile and heat transfer rate decrease in the order of platelet, cylinder, blade, brick, and sphere shape, respectively. The heat transfer rate of platelet-shaped nanoparticles have higher(4.90% than cylinder-shaped nanoparticles, 5.16% than blade-shaped nanoparticles, 9.22% than brick-shaped nanoparticles, 10.57% than sphere-shaped nanoparticle) for fixed values of various parameters. A rise in radiation parameter and viscosity parameter increases heat transfer rate.

Keywords: stretching sheet, nanoparticles shapes, partial slip, MHD flow, radiation parameter, variable viscosity, thermal conductivity.

Submitted: 26 March 2026
Accepted: 26 April 2026
Published: 06 May 2026

Vol. 2, **No.** 2, 2026.
10.62762/JAM.2026.636964

***Corresponding author:**
Ravi Gupta
rgupta@vmou.ac.in

Citation
Kumar, B., & Gupta, R. (2026). Heat Transfer and Thermal Radiation Inspection of MHD Flow of Hybrid Nanofluid with Variable Viscosity and Thermal Conductivity Using Various Shapes. *ICCK Journal of Applied Mathematics*, 2(2), 173–194.

List of symbols

U_{w}	Velocity near the sheet $(\mathrm{m.s^{-1}})$
c	Stretching constant $(\mathrm{s^{-1}})$
t	Time (s)
T_{w}	Temperature near the surface (K)
T_{∞}	Ambient temperature (K)
T_{r}	Reference temperature (K)
ϵ	Thermal conductivity parameter (-)
B_0	Applied magnetic field strength $(\mathrm{kg.s^{-2}.A^{-1}})$
F	Velocity slip coefficient (m)
w_0	Suction velocity $(\mathrm{m.s^{-1}})$
q_r	Radiative heat flux $(\mathrm{kg.s^{-3}})$
Q_0	Heat generation per unit volume per unit temperature $(\mathrm{kg.m^{-1}.s^{-3}.K^{-1}})$
c_p	Specific heat at constant pressure $(\mathrm{m^2.s^{-2}.K^{-1}})$
Nu	Nusselt number (-)
M	Magnetic parameter (-)
ν_{f}	Kinematic viscosity $(\mathrm{m^2.s^{-1}})$
C_f	Skin friction coefficient (-)
k	Thermal conductivity $(\mathrm{kg.m.s^{-3}.K^{-1}})$
$f(\eta)$	Dimensionless stream function (-)
F_w	Suction parameter (-)
α	Unsteadiness constant $(\mathrm{s^{-1}})$
N_s	Slip parameter (-)
μ	Coefficient of viscosity $(\mathrm{kg.m^{-1}.s^{-1}})$
J	Unsteadiness parameter (-)
σ	Electrical conductivity $(\mathrm{S.m^{-1}})$
R	Viscosity parameter (-)
σ^*	Stefan-Boltzmann constant $(\mathrm{kg.s^{-3}.K^{-4}})$
k^*	Mean absorption coefficient $(\mathrm{m^{-1}})$
ρ	Fluid density $(\mathrm{kg.m^{-3}})$
Bi	Biot number (-)
Pr_{v}	Variable Prandtl number (-)
Ra	Radiation parameter (-)
$\frac{c}{(1-\alpha t)}$	Stretching rate $(\mathrm{s^{-1}})$
g_s	Surface heat transfer coefficient $(\mathrm{W.m^{-2}.K^{-1}})$
E_k	Eckert number (-)

1 Introduction

The study of heat transfer and thermal radiation inspection for various shapes of hybrid nanoparticles with variable viscosity and thermal conductivity has wide applications in heat exchanging system, solar system, textile industries, nuclear reactors, gas turbines, chemical industries, biological sensing, medicine, and in many technology. This study design for higher efficient thermal systems such as cooling in nuclear plants, heat exchangers in industries for concentrated solar power, reducing design uncertainty, lowers operational energy use and cost, lowest carbon energy infrastructure. This study improves thermal control in magnetically driven pumps, heat exchangers and solar receiver. It gives us some social-economic benefits such as reduced energy consumption, lower emissions, increase the reliability of supply chain in energy-intensive reactors and improved equipment longevity. The presence of variable magnetic field gives rise into Joule heating, which generates thermal energy in electrically conducting fluid. Heat generation parameter useful into nuclear processes, chemical reactions, and other energy sources. We are using PAO oil base fluid which is highly viscous and viscous dissipation converts mechanical energy into heat. Thermal radiation is important in heat transfer processes such as solar collectors and furnaces. A slip condition included because of nanoparticle collision on boundary surface. Convective boundary condition is necessary when surface is heated and cooled by another fluid. According to Choi et al. [1], nanofluid enhanced the thermal conductivity compared to normal fluid. Saeed et al. [2] examined thermal radiation effect with slip into porous medium for darcy-forchheimer hybrid nanofluid flow. Zeeshan et al. [3] studied about heat transfer of MHD thin film flow of $(\mathrm{Cu}-\mathrm{Al_2O_3})$/ethylene glycol hybrid nanofluid along a surface which is stretchable permeable sheet. Gupta et al. [4] investigated about marangoni convection MHD flow for distinct nanofluids along a stretching surface under the effects of thermal radiation. Dadheech et al. [5] discussed about entropy analysis in different fluid with radiative slip flow into porous media. Turkyilmazoglu et al. [6] investigated stagnation point flow for moving permeable flat surface with time dependent magnetic field. Iqbal et al. [7] analysed about heat transfer enhancement for various shape nanoparticles using (ethylene glycol-Cu) nanofluid through a sheet, which is radially stretching. They found that the highest flow and heat transfer rate were noticed for platelet and sphere shape nanoparticles, respectively. Jangid et al. [8] studied about heat and mass transfer with radiation, suction effect by using exponentially stretched surface for williamson nanofluid. Shahzad et al. [9] studied on generalized lubrication theory for squeeze fluid film with non linearly stretching/shrinking boundaries. Kumar et al. [10] illustrated unsteady rotational motion of spherical particles with slip condition. Two different models were used by Turkyilmazoglu [11] for heat and fluid flow analysis over stretching and shrinking sheet. Ali et al. [12] investigated about silica nanofluid flow along a unsteady stretching cylinder for various shape of nanoparticles with joule heating effect. Rafique et al. [13] investigated about filtration problem of two dimensional incompressible, Newtonian and viscous fluid flow over a permeable walled tube. Yahaya et al. [14] studied the influence of slip condition into a long channel connect by large reservoirs. Patel et al. [15] investigated hybrid nanofluid flow with coupled nonthermal plasma over a photocatalytic surface. A non-newtonian hybrid nanofluid utilised to investigate of enhancing thermal performance and assessing heat absorption, which was discussed by Yusuf et al. [16]. The study of Time-dependent rotational motion for Jeffrey fluid using Laplace transform was studied by kumar and Madasu [17].

Ragavi and Poornima[18] analysed about heat transfer of $(\mathrm{Ag}-\mathrm{Al_2O_3}/\mathrm{water})$ MHD hybrid nanofluid flow using different shapes of nanoparticles with suction and partial slip parameter. The theoretically study on nanofluid with slip conditions and thermal radiation was discussed by Yusuf et al. [19] in solar panels. The computational study on graphene oxide/vacuum residue nanofluid was done by Yang et al. [20], for enhancing oil recovery. Mahmood et al. [21] investigated about tetra hybrid nanofluid through a shrinking cylinder taking variable viscosity and electrical conductivity with suction and thermal radiation effect. Abdulhakeem Yusuf et al [22] investigated heat transfer of MWCNT-$\mathrm{Al_2O_3}$ hybrid nanofluid. By considering variable viscosity, the impact of viscous dissipation of unsteady incompressible flow of $(\mathrm{Al_2O_3}-\mathrm{CuO})$/water hybrid nanofluid including thermal radiation was discussed by Famakinwa et al [23]. By considering particle shape effect, the study about heat transfer and flow of Ag-nanoparticles along a stretching surface was illustrated by Hayat et al. [24]. Kumar and Gupta[25] investigated heat transfer of hybrid nanofluid using nonlinear PDEs. Makinde et al. [26] investigated about heat transfer and flow structure of $(\mathrm{TiO_2}$-PAO oil) nanofluid in a microchannel considering variable viscosity. Ferdows et al. [27] analysed about heat transfer of MHD hybrid nanofluid for a moving thin needle taking variable thermal conductivity and viscosity. Manigandan and Narayana[28] investigated about heat transfer of hybrid nanofluid considering variable viscosity and thermal conductivity.

After comprehensive review of the literature, we have observed that several analytical studies have been done by researchers on hybrid nanofluid and their properties with different geometry and configuration. In previous published work on hybrid nanofluid, many studies have been done assuming viscosity and thermal conductivity as constant throughout the fluid motion, and also they assumed no slip condition. As we know, when we give external heat to hybrid nanofluid then the viscosity and thermal conductivity will not remain constant and it depends on temperature. Also, nanoparticles slip on boundary due to nanoparticles collision. As far as literature review has been done by us, we didn't find any study on how different shapes of nanoparticles influence the fluid flow in the presence of variable viscosity and thermal conductivity with thermal radiation. These are all gaps in previous study which was not accomplished.

To fulfil these gaps we investigate about heat transfer and thermal radiation inspection of$(\mathrm{Ag}-\mathrm{TiO_2}/\mathrm{PAO}$ oil) hybrid nanofluid for different shapes of nanoparticles along a unsteady radially stretching sheet taking variable thermal conductivity and viscosity. In this current investigation we have explore platelet, sphere, brick, blade, cylinder shaped nanoparticles. The impact of external heat generation and internal friction on viscosity and thermal conductivity are investigates. The impact of slip and suction is also included for controlling thermal transport circumstance. We are taking $\mathrm{Ag}-\mathrm{TiO_2}$ hybrid nanoparticles in our study because melting point of Ag and $\mathrm{TiO_2}$ nanoparticles are higher than boiling point of PAO oil, that's why Ag and $\mathrm{TiO_2}$ have not melt in base fluid PAO oil. We also used PAO oil as a base fluid because the viscosity of PAO oil is higher compared to all other base fluid(water, EG, PG, Kerosene oil). This combination of Ag and $\mathrm{TiO_2}$ nanoparticles with PAO oil gives us better results to understand the heat transfer and velocity concept in the presence of variable viscosity and thermal conductivity. For that we formulate fluid flow equations and, the governing equations are resolved through BVP4C method. The consequences are shown through numerous graphs and tables for different shapes of nanoparticles and thermal observations. Also analysis of various physical parameters namely radiation(Ra), internal heat generation(Q), thermal conductivity parameter(ϵ), unsteadiness parameter(J), viscous dissipation(E_k), prandtl number(Pr_{v}), magnetic parameter(M), viscosity parameter(R) on velocity, temperature, skin friction and nusselt number is discussed.

2 Problem Formulation

Consider the unsteady radially stretching sheet with two dimensional boundary layer flow of hybrid nanofluid $(\mathrm{Ag}-\mathrm{TiO_2}/\mathrm{PAO\ Oil})$ for different shapes of (Ag) and $(\mathrm{TiO_2})$ nanoparticles. The radial velocity of stretching sheet is $U_\mathrm{w} = \frac{cr}{(1-\alpha t)}$ [18]. The sheet is considered in $z=0$ plane with cylindrical coordinates (r,θ,z). The physical configuration of the problem is shown in Figure 1. In this MHD flow viscosity and thermal conductivity of hybrid nanofluid are dependent function of temperature. Also, suction and partial slip conditions are considered and surface temperature is $T_\mathrm{w} = T_\infty + T_\mathrm{r}\left(\frac{cr^2}{2\nu_f}\right)(1-\alpha t)^{-\frac{3}{2}}$ [18] and $T_\mathrm{w} - T_\infty > 0$ is considered. A time dependent magnetic field $B = \frac{B_0}{\sqrt{1-\alpha t}}$ [18] is applied on sheet which is perpendicular to surface. The velocity profile is $v(r,z) = (u,0,w)$, where $u(r,z)$ and $w(r,z)$ are longitude and transverse components of velocity across the radial and axial direction.

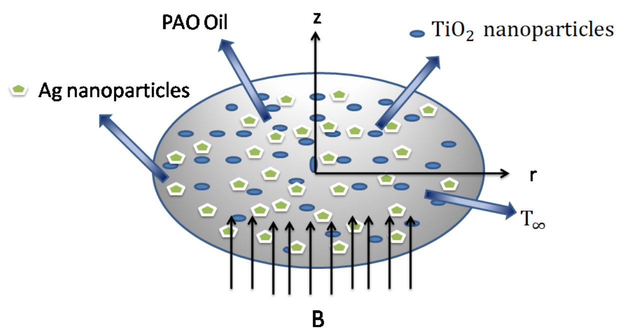

Figure 1. Flow geometry for hybrid nanofluid along stretching sheet

In this above assumption the governing equations can be written as follow [18, 23, 27]

$$\frac{\partial u}{\partial r} + \frac{\partial w}{\partial z} + \frac{u}{r} = 0, \tag{1}$$

$$\frac{\partial u}{\partial t} + u\frac{\partial u}{\partial r} + w\frac{\partial u}{\partial z} = \frac{1}{\rho_\mathrm{hnf}}\frac{\partial}{\partial z}\left(\mu_\mathrm{hnf}(T)\frac{\partial u}{\partial z}\right) - \frac{\sigma_\mathrm{hnf}}{\rho_\mathrm{hnf}}B^2(r,t)u, \tag{2}$$

$$\frac{\partial T}{\partial t} + u\frac{\partial T}{\partial r} + w\frac{\partial T}{\partial z} = \frac{1}{(\rho c_p)_\mathrm{hnf}}\frac{\partial}{\partial z}\left(k_\mathrm{hnf}(T)\frac{\partial T}{\partial z}\right) + \frac{\mu_\mathrm{hnf}(T)}{(\rho c_p)_\mathrm{hnf}}\left(\frac{\partial u}{\partial z}\right)^2 + \frac{\sigma_\mathrm{hnf}}{(\rho c_p)_\mathrm{hnf}}B^2(r,t)u^2 + \frac{Q_0}{(\rho c_p)_\mathrm{hnf}}(T-T_\infty) - \frac{1}{(\rho c_p)_\mathrm{hnf}}\frac{\partial q_r}{\partial z}, \tag{3}$$

The subject to the following boundary conditions are represented as follow [18]

$$\begin{aligned} \text{at z = 0 ;} \qquad & u = U_\mathrm{w} + F\frac{\partial u}{\partial z}, \\ & w = w_0, \\ & -k_\mathrm{hnf}(T)\frac{\partial T}{\partial z} = g_s(T_\mathrm{w} - T), \\ z \to \infty \qquad & u \to 0, \quad T \to T_\infty, \end{aligned} \tag{4}$$

In boundary conditions (4), at the wall surface first, velocity slip condition imposed for finite fluid slip effect. second, suction condition to control the boundary-layer thickness. Third, the convective boundary condition which indicates heat is transferred to the surface by another hot fluid with heat transfer coefficient. For far away from surface, the fluid velocity zero indicate free stream velocity and temperature tend to ambient fluid temperature.

The variable viscosity defined by Reynolds model, which is given by [23]

$$\mu_\mathrm{hnf}(T) = \mu_\mathrm{hnf}\exp(-R\theta(\eta)), \tag{5}$$

Expanding (5) by Maclaurin series, with ignoring higher order terms we get

$$\mu_\mathrm{hnf}(T) = \mu_\mathrm{hnf}\left(1 - R\theta(\eta) + \frac{R^2\theta^2(\eta)}{2}\right), \tag{6}$$

The variable thermal conductivity of hybrid nanofluid defined as follow [27]

$$k_\mathrm{hnf}(T) = k_\mathrm{hnf}(1 + \epsilon\theta(\eta)), \tag{7}$$

where $R > 0$ and $\epsilon > 0$ are viscosity parameter and thermal conductivity parameter, respectively.

The Rosseland diffusion approximation approximation known as follow [23]

$$q_r = -\frac{4\sigma^*}{3k^*}\frac{\partial T^4}{\partial z}, \tag{8}$$

Expanding T^4, by Taylor series, with ignoring higher order terms we get

$$T^4 \equiv T_\infty^3[4T - 3T_\infty]. \tag{9}$$

By equations (8) and (9)

$$q_r = -\frac{16T_\infty^3\sigma^*}{3k^*}\frac{\partial T}{\partial z}. \tag{10}$$

Thermophysical properties of hybrid nanoparticles $(Ag-TiO_2)$ into base fluid poly-alpha-olefin oil are [18]

$$\rho_{\text{hnf}} = (1-\phi_1-\phi_2)\rho_{\text{f}} + \phi_1\rho_{\text{s}_1} + \phi_2\rho_{\text{s}_2},$$
$$\mu_{\text{hnf}} = \mu_{\text{f}}(1+w_1\phi_1+w_2\phi_1^2)(1+w_1\phi_2+w_2\phi_2^2),$$
$$(\rho c_p)_{\text{hnf}} = (1-\phi_1-\phi_2)(\rho c_p)_{\text{f}} + \phi_1(\rho c_p)_1 + \phi_2(\rho c_p)_2,$$
$$\sigma_{\text{hnf}} = \sigma_{\text{f}}\left(1+\frac{3(\frac{\sigma_{\text{s}2}}{\sigma_{\text{f}}}-1)\phi_2}{(\frac{\sigma_{\text{s}2}}{\sigma_{\text{f}}}+2)-(\frac{\sigma_{\text{s}2}}{\sigma_{\text{f}}}-1)\phi_2}\right)\times \left(1+\frac{3(\frac{\sigma_{\text{s}1}}{\sigma_{\text{f}}}-1)\phi_1}{(\frac{\sigma_{\text{s}1}}{\sigma_{\text{f}}}+2)-(\frac{\sigma_{\text{s}1}}{\sigma_{\text{f}}}-1)\phi_1}\right),$$
$$\frac{k_{\text{hnf}}}{k_{\text{f}}} = \frac{k_{\text{s}_2}+(n-1)k_{\text{f}}+(n-1)(k_{\text{s}_2}-k_{\text{f}})\phi_2}{k_{\text{s}_2}+(n-1)k_{\text{f}}-(k_{\text{s}_2}-k_{\text{f}})\phi_2}\times \frac{k_{\text{s}_1}+(n-1)k_{\text{f}}+(n-1)(k_{\text{s}_1}-k_{\text{f}})\phi_1}{k_{\text{s}_1}+(n-1)k_{\text{f}}-(k_{\text{s}_1}-k_{\text{f}})\phi_1}, \tag{11}$$

where ϕ_1, ϕ_2 denotes as Ag and TiO_2 nanoparticles volume fractions and σ_{hnf}, μ_{hnf}, ρ_{hnf}, k_{hnf}, $(\rho c_p)_{\text{hnf}}$ are electrical conductivity, dynamic viscosity, density, thermal conductivity and heat capacity of hybrid nanofluid, respectively. The subscripts hnf, f, s_1, s_2 denotes as hybrid nanofluid, base fluid, first nanoparticle (Ag) and second nanoparticle (TiO_2). n is the shape factor for various nanoparticle geometries and w_1 and w_2 are viscosity heat capacitance coefficient.

Using various dimensionless variables and transformations as [18]

$$\psi = \frac{r^2 U_{\text{w}} f(\eta)}{\sqrt{Re}},\quad \theta(\eta) = \frac{T-T_\infty}{T_{\text{r}}\left(\frac{cr^2}{2\nu_{\text{f}}}\right)(1-\alpha t)^{-\frac{3}{2}}},\quad \eta = \frac{z\sqrt{Re}}{r},\quad Re = \frac{rU_{\text{w}}}{\nu_{\text{f}}}, \tag{12}$$

where η is independent variable and Re, ψ are represent as reynolds number and stream function respectively.

$$u = -\frac{1}{r}\frac{\partial\psi}{\partial z} = U_{\text{w}} f'(\eta),\quad w = \frac{1}{r}\frac{\partial\psi}{\partial r} = -2U_{\text{w}} Re^{-\frac{1}{2}} f(\eta), \tag{13}$$

Equations (2) and (3) transformed into non linear ordinary differential equations by equations (12) and (13), which is given by

$$\frac{A_1}{A_3}\left(1-R\theta+\frac{R^2\theta^2}{2}\right)f''' - M\frac{A_4}{A_3}f' - \frac{A_1}{A_3}R\theta' f'' + \frac{A_1}{A_3}R^2\theta\theta' f'' - (f')^2 - J\left(\frac{\eta}{2}f''+f'\right) + 2ff'' = 0, \tag{14}$$

$$\frac{A_1(1-R\theta+\frac{R^2\theta^2}{2})(A_2(1+\epsilon\theta)+Ra)}{A_2A_5(1+\epsilon\theta)Pr_{\text{v}}}\theta'' + \frac{A_4}{A_5}ME_k(f')^2 - \left(\frac{J}{2}(3\theta+\eta\theta')+2\theta f'-2f\theta'\right) + \frac{A_1}{A_5}\frac{\epsilon(1-R\theta+\frac{R^2\theta^2}{2})}{(1+\epsilon\theta)Pr_{\text{v}}}(\theta')^2 + \frac{Q.\theta}{A_5} + \frac{A_1}{A_5}E_k\left(1-R\theta+\frac{R^2\theta^2}{2}\right)(f'')^2 = 0, \tag{15}$$

The reduced boundary conditions are

$$f(\eta) = F_w,\quad f'(\eta) = (1+N_s f''(\eta)),\quad \theta'(\eta) = -\frac{Bi}{A_2}\frac{(1-\theta(\eta))}{(1+\epsilon\theta(\eta))}\quad \text{at } \eta = 0; \quad f'(\eta)\to 0,\quad \theta(\eta)\to 0,\quad as\ \ \eta\to\infty; \tag{16}$$

The constants A_1, A_2, A_3, A_4 and A_5 are defined as

$$A_1 = \frac{\mu_{\text{hnf}}}{\mu_{\text{f}}}, A_2 = \frac{k_{\text{hnf}}}{k_{\text{f}}}, A_3 = \frac{\rho_{\text{hnf}}}{\rho_{\text{f}}},\quad A_4 = \frac{\sigma_{\text{hnf}}}{\sigma_{\text{f}}}, A_5 = \frac{(\rho c_p)_{\text{hnf}}}{(\rho c_p)_{\text{f}}} \tag{17}$$

Several dimensionless constants are as follows: $E_k = \frac{2\nu_{\text{f}} c}{T_{\text{r}} c_p\sqrt{1-\alpha t}}$ is Eckert number, $J = \frac{\alpha}{c}$ is unsteadiness parameter, $Pr_{\text{v}} = \frac{(c_p)_{\text{f}}\mu_{\text{hnf}}(T)}{k_{\text{hnf}}(T)}$ refers to variable Prandtl number, $N_s = F\sqrt{\frac{c}{\nu_{\text{f}}(1-\alpha t)}}$ is Slip parameter, $M = \frac{B_0^2\sigma_{\text{f}}}{c\rho_{\text{f}}}$ is Magnetic parameter, $F_w = -\frac{w_0}{2}\sqrt{\frac{(1-\alpha t)}{c\nu_{\text{f}}}}$ refers to suction parameter, $Bi = \frac{g_s}{k_{\text{f}}}\sqrt{\frac{\nu_{\text{f}}(1-\alpha t)}{c}}$ is Biot number, $Ra = \frac{16\sigma^* T_\infty^3}{3k^* k_{\text{f}}}$ is Radiation parameter, $Q = \frac{Q_0(1-\alpha t)}{c(\rho c_p)_{\text{f}}}$ is heat generation coefficient, R refers to viscosity parameter and ϵ is thermal conductivity parameter.

The local nusselt number(Nu) and the local skin friction coefficient(C_f) are defined as [18]

$$C_f = \frac{\tau_{\text{w}}}{\rho_{\text{f}} U_{\text{w}}^2},\qquad Nu = \frac{rq_w}{k_{\text{f}}(T_{\text{w}}-T_\infty)} \tag{18}$$

where $\tau_{\text{w}} = \mu_{\text{hnf}}(T)\left(\frac{\partial u}{\partial z}\right)_{z=0}$ and $q_w = -k_{\text{hnf}}(T)\left(\frac{\partial T}{\partial z}\right)_{z=0} + q_r$ are shear stress and wall heat flux on sheet surface, respectively and equation (18) can be transformed into the following form:

$$\begin{aligned} C_f Re^{\frac{1}{2}} &= \frac{\mu_{\text{hnf}}}{\mu_{\text{f}}}\left(1 - R\theta + \frac{R^2\theta^2}{2}\right) f''(0) \\ Nu Re^{\frac{-1}{2}} &= -\left(\frac{k_{\text{hnf}}}{k_{\text{f}}}(1+\epsilon\theta) + Ra\right)\theta'(0) \\ &= -\big(A_2(1+\epsilon\theta) + Ra\big)\theta'(0) \end{aligned} \tag{19}$$

3 Solution procedure

The consequence non linear ordinary differential equations (14) and (15) along with boundary conditions (16) are solved by numerically technique BVP4C making use of MATLAB. The detailed numerical computational procedure is discussed in Appendix A.

Appendix A : Numerical solution Procedure

We are converteing all equations into the 1^{st} order differential equation. For that we use following substitutions

$$\begin{aligned} f &= y(1), \\ f' &= y(2), \\ f'' &= y(3), \\ f''' &= \frac{A_3}{A_1\left(1 - Ry(4) + \frac{R^2(y(4))^2}{2}\right)}\Bigg(\frac{MA_4}{A_3}y(2) \\ &+ \frac{RA_1}{A_3}y(3)y(5) - \frac{R^2A_1}{A_3}y(3)y(4)y(5) + (y(2))^2 \\ &+ J\big(y(2) + \frac{\eta}{2}y(3)\big) - 2y(3)y(1)\Bigg), \\ \theta &= y(4), \\ \theta' &= y(5), \\ \theta'' &= \frac{A_2A_5Pr_{\text{v}}(1+\epsilon\theta)}{A_1\left(1 - Ry(4) + \frac{R^2(y(4))^2}{2}\right)\big(A_2(1+\epsilon y(4)) + Ra\big)} \\ &\Bigg[\frac{J}{2}\big(\eta y(5) + 3y(4)\big) + 2y(4)y(2) - 2y(5)y(1) \\ &- \frac{Qy(4)}{A_5} - \frac{\epsilon A_1\left(1 - Ry(4) + \frac{R^2(y(4))^2}{2}\right)}{Pr_{\text{v}}(1+\epsilon\theta)A_5}(y(5))^2 \\ &- \tfrac{A_1}{A_5}E_k\left(1 - Ry(4) + \tfrac{R^2(y(4))^2}{2}\right)(y(3))^2 - \tfrac{A_4}{A_5}ME_k(y(2))^2\Bigg], \end{aligned}$$

and boundary conditions are

$$\begin{aligned} y_1(0) &= F_w, \quad y_2(0) = [1 + N_s y_3(0)], \\ y_5(0) &= -\frac{Bi}{A_2}\frac{(1 - y_4(0))}{(1+\epsilon y_4(0))}, \\ y_2(\infty) &\to (0), \quad y_4(\infty) \to (0) \end{aligned}$$

4 Results and discussion

Table 1. Thermophysical values of hybrid nanoparticles and base fluids [18, 26].

Physical Characters	Ag	TiO_2	PAO oil
Thermal Conductivity $K(\frac{W}{mK})$	429	8.9538	0.143
Specific heat $c_p(\frac{J}{Kg.K})$	235	686.2	2303
Electrical Conductivity $\sigma(\frac{S}{m})$	62.1×10^6	0.125	1.0×10^{-8}
Density $\rho(\frac{Kg}{m^3})$	10500	4250	798

Table 2. Visualization of viscosity coefficient and shape factor of nanoparticles [24].

Shape	Sphere	Brick	Blade	Cylinder	Platelet
w_1	2.5	1.9	14.6	13.5	37.1
w_2	6.5	471.4	123.3	904.4	612.6
n	3	3.72	8.26	4.82	5.72

The main attention is to find out the impact of different non dimensional parameters on velocity and temperature profile for various shape (Platelet, Cylinder, Blade, Brick, Sphere) of $(Ag - TiO_2)$ hybrid nanoparticles into Poly-alpha-olefin oil base fluid taking variable thermal conductivity and viscosity. We are considering various non dimensional parameters such as solid volume fraction(ϕ), biot number(Bi), Eckert number(E_k), external heat generation parameter(Q), magnetic parameter(M), prandtl number(Pr_{v}), slip parameter(N_s), viscosity parameter(R), suction parameter(F_w), unsteadiness parameter(J), thermal conductivity parameter(ϵ) and radiation parameter(Ra). The consequences are shown through plotted graphs and tables and also, the impact of Nusselt number and skin Friction are examined through tables. The physical parameters

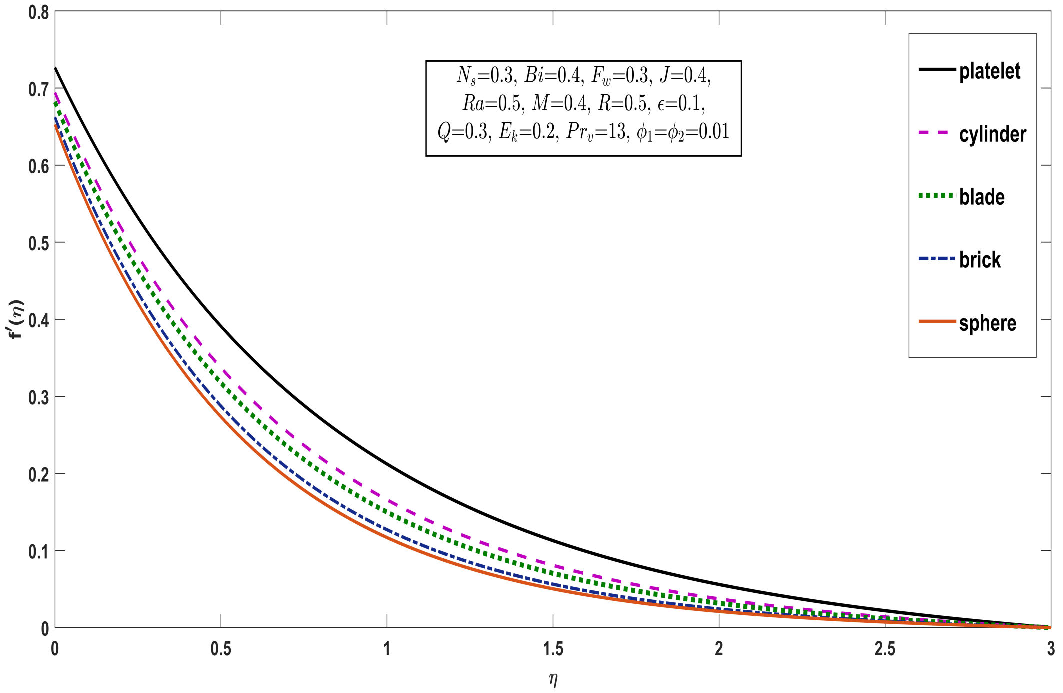

Figure 2. Influence of velocity distribution for various shapes of nanoparticles.

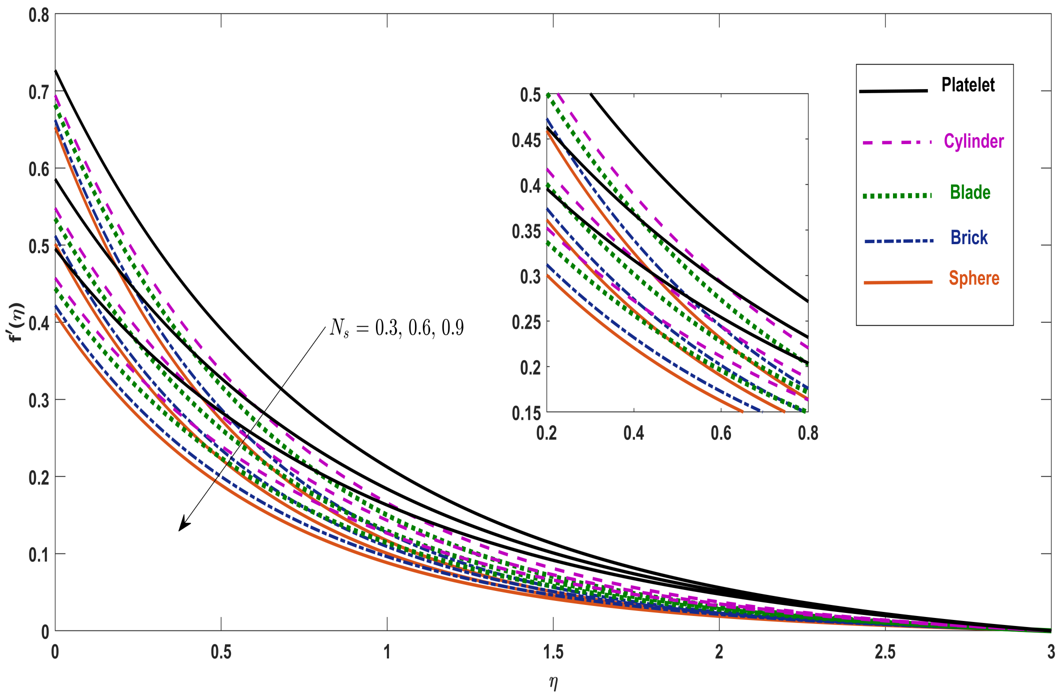

Figure 3. Influence on velocity with slip parameter(N_s).

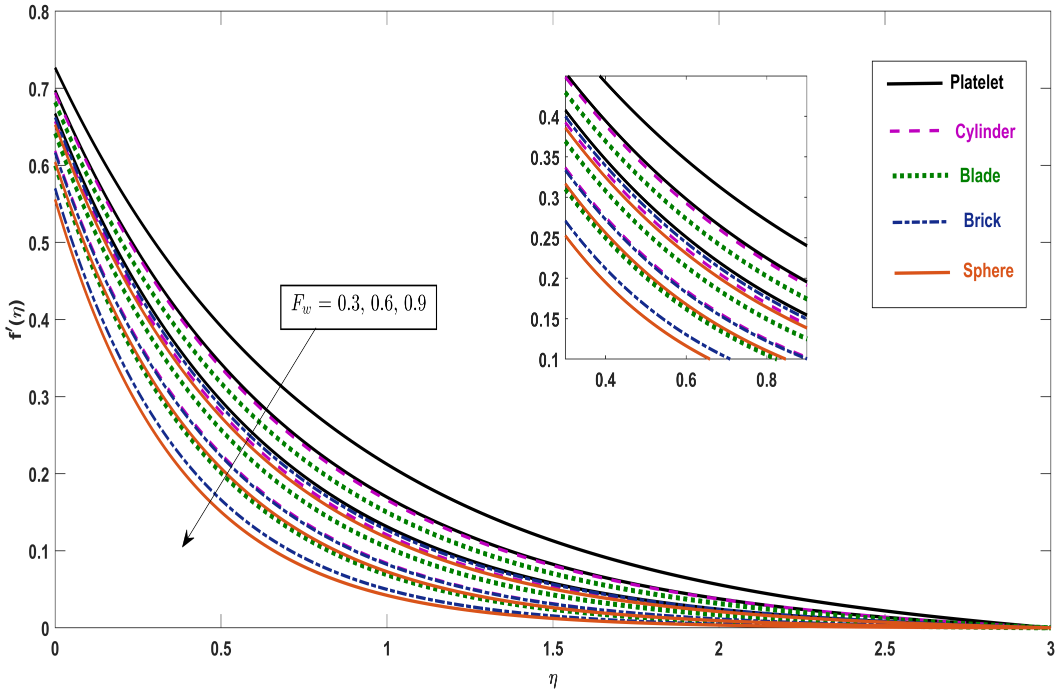

Figure 4. Influence on velocity with suction parameter(F_w).

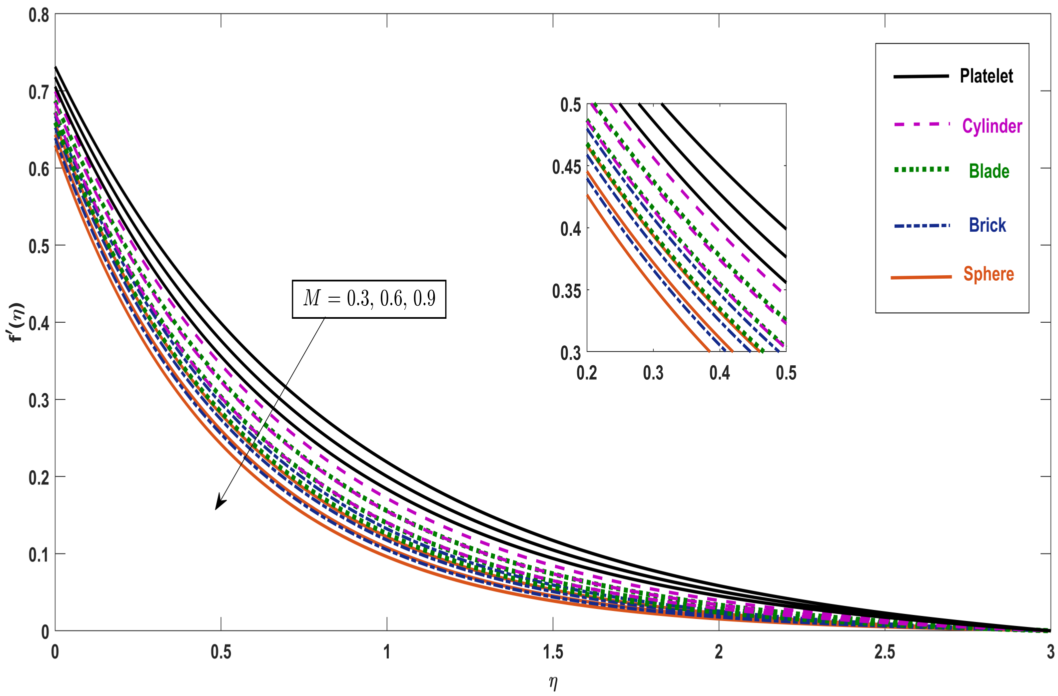

Figure 5. Influence on velocity with magnetic parameter(M).

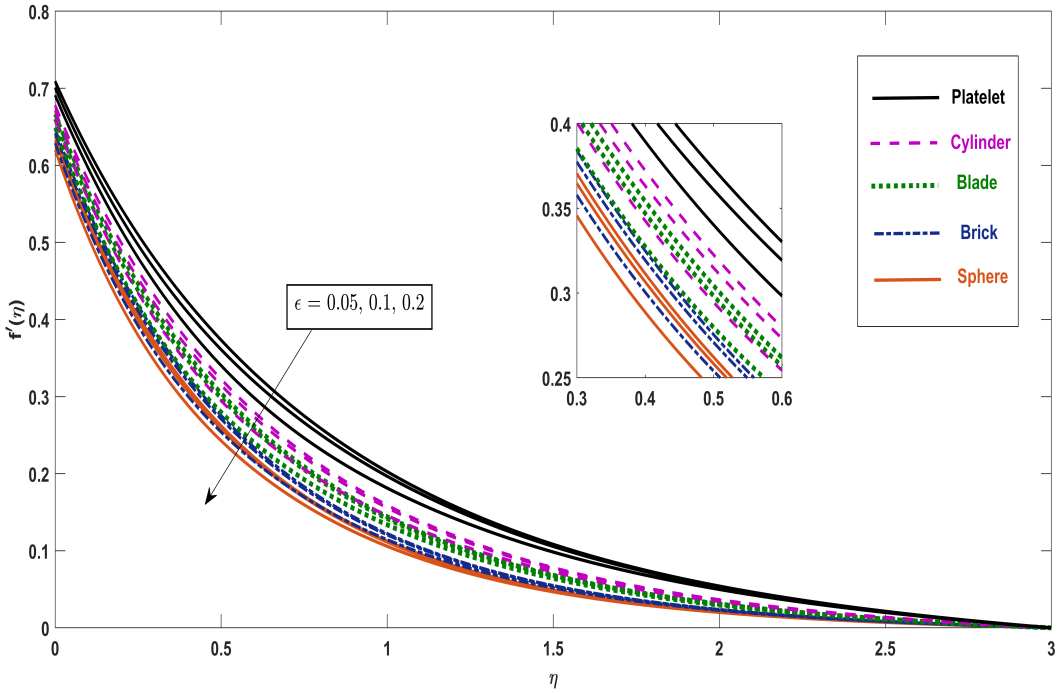

Figure 6. Influence on velocity with thermal conductivity parameter(ϵ).

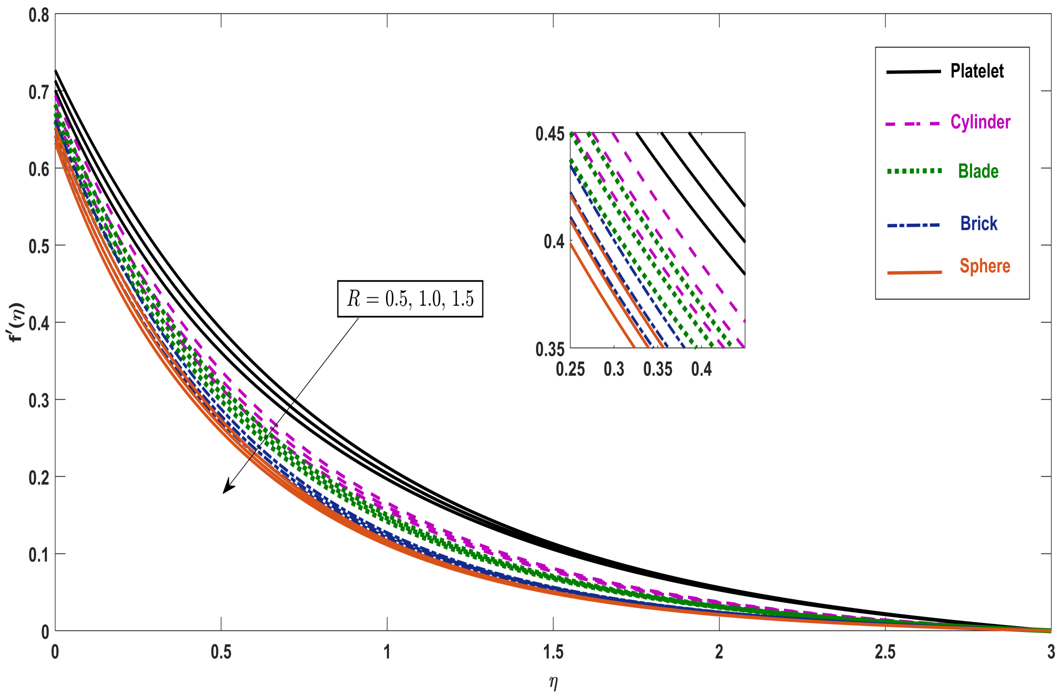

Figure 7. Influence on velocity with viscosity parameter(R)

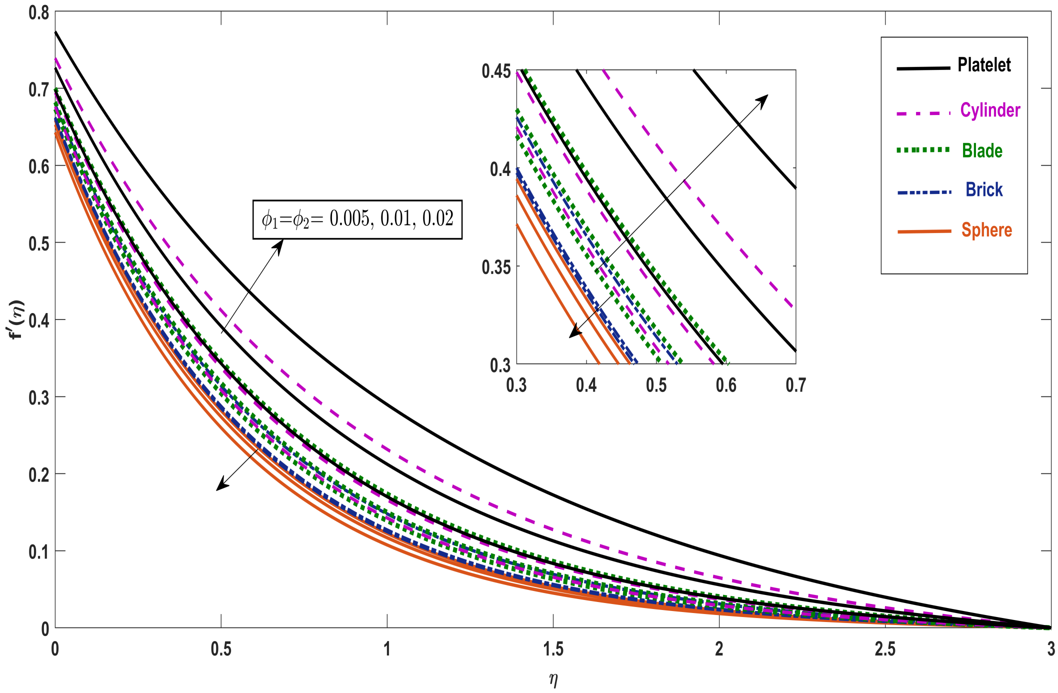

Figure 8. Influence on velocity with volume fractions on nanoparticles(ϕ_1 and ϕ_2).

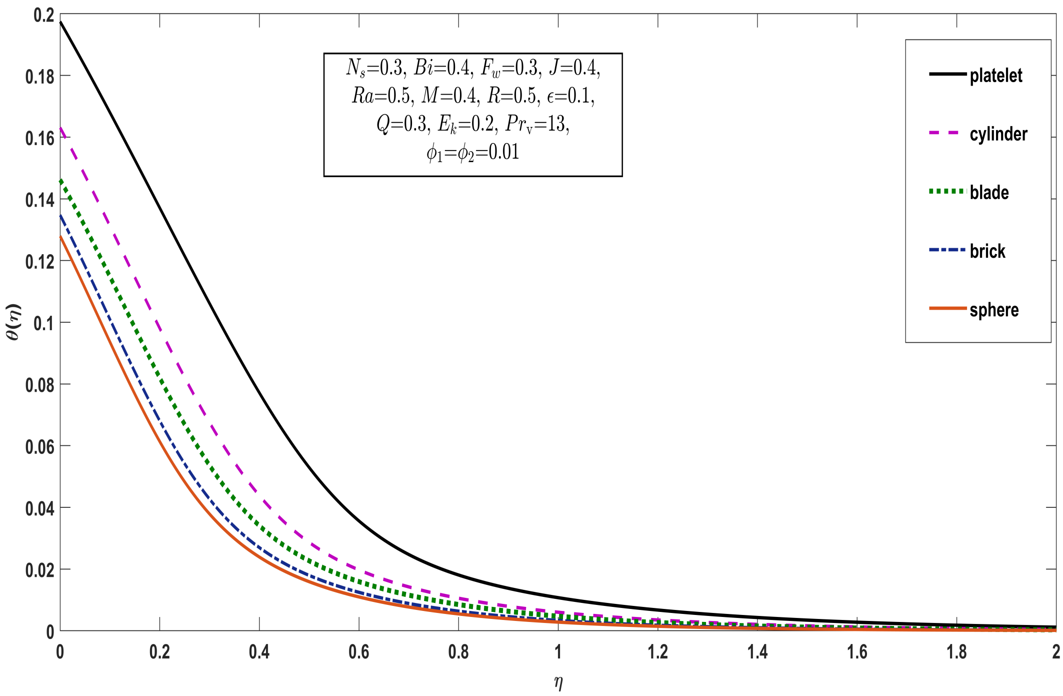

Figure 9. Influence of temperature distribution for various shape of nanoparticles.

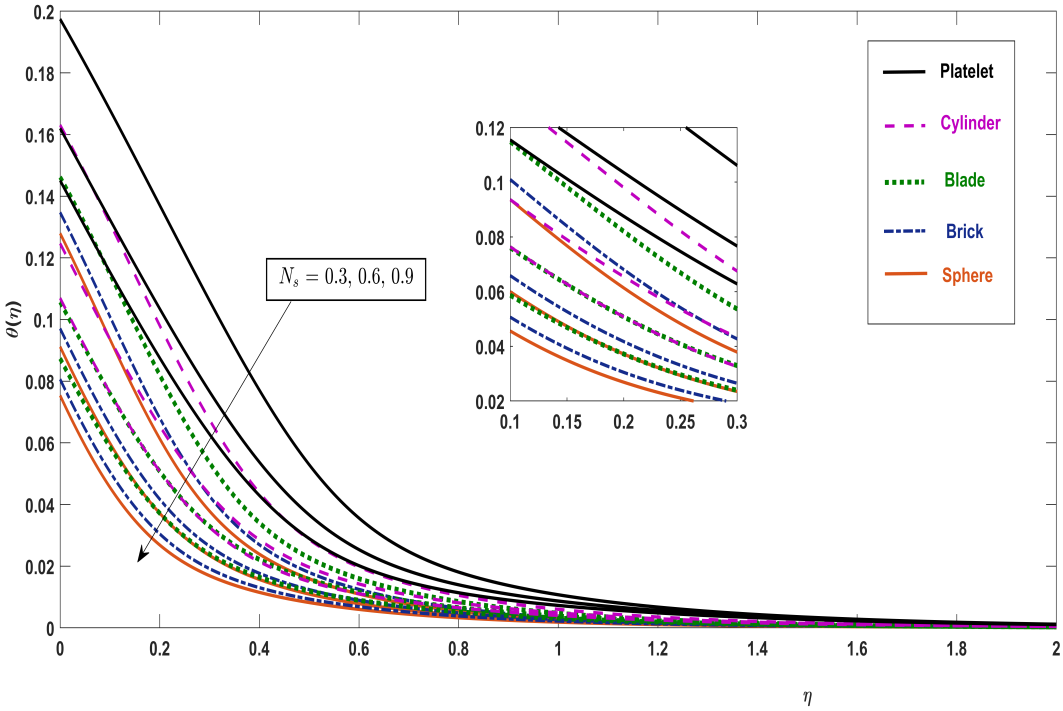

Figure 10. Influence on temperature with slip parameter(N_s).

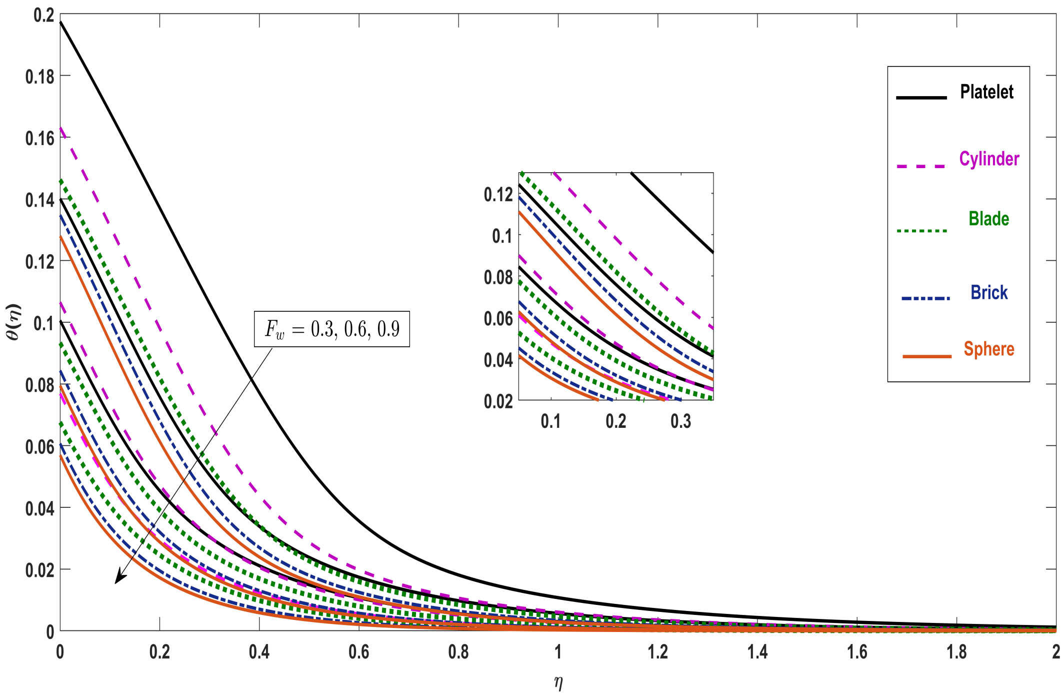

Figure 11. Influence on temperature with suction parameter(F_w).

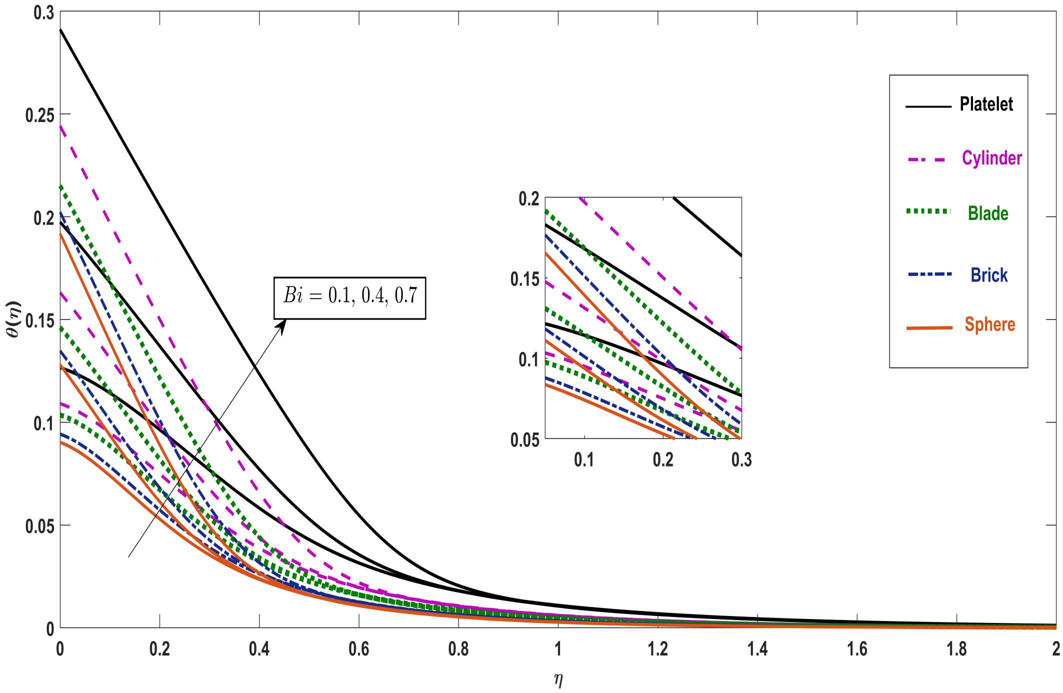

Figure 12. Influence on temperature with biot number(Bi).

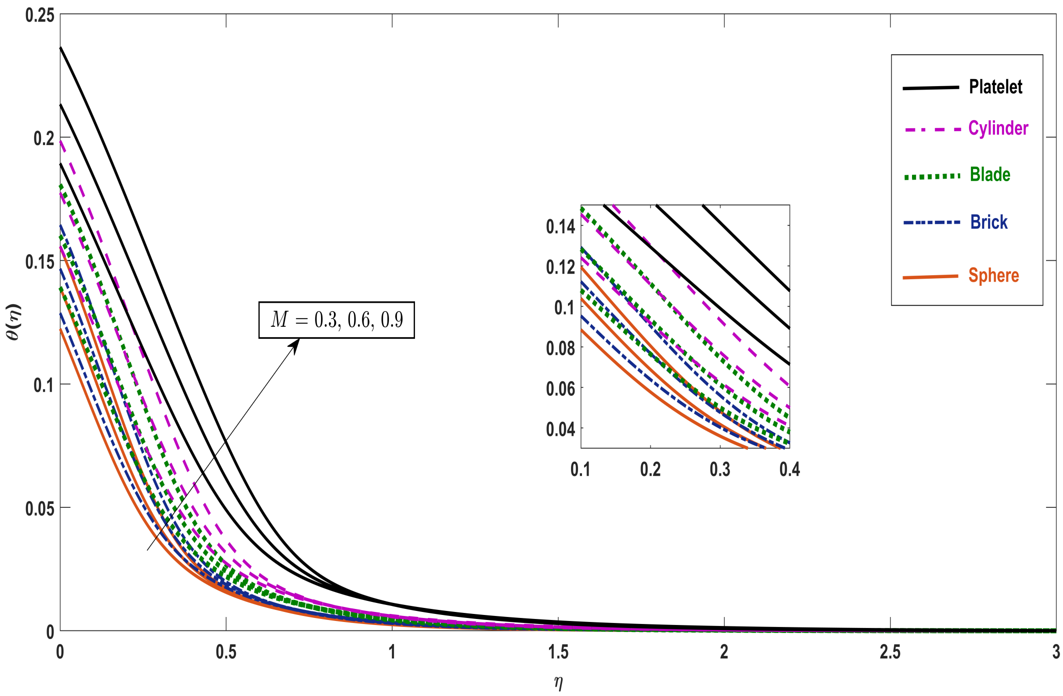

Figure 13. Influence on temperature with magnetic parameter(M).

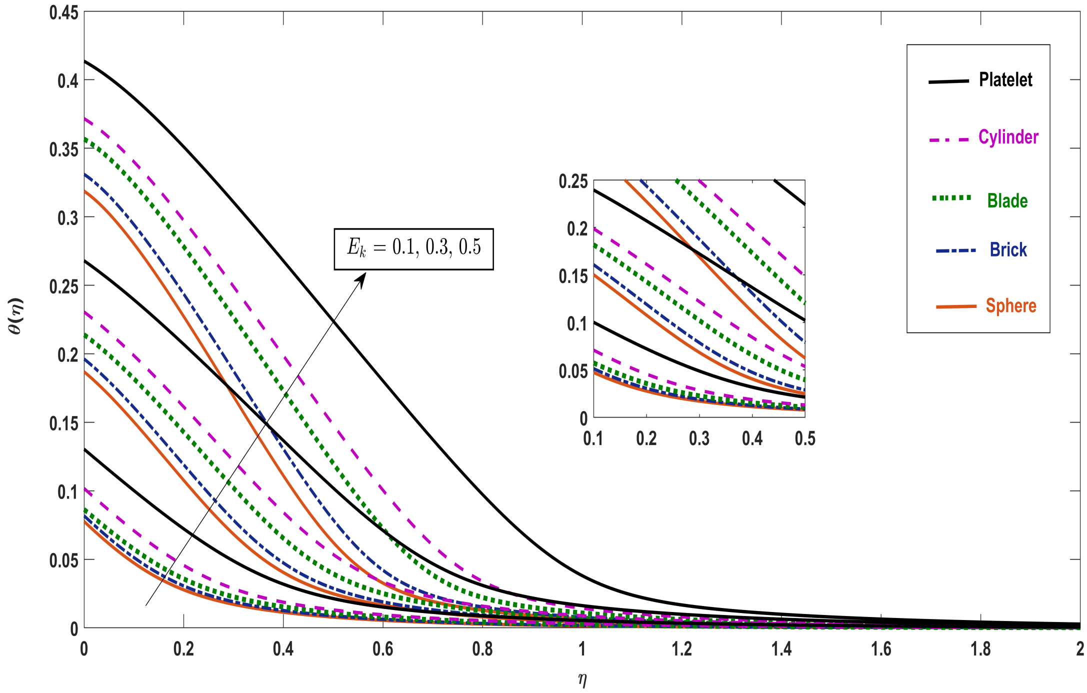

Figure 14. Influence on temperature with eckert number(E_k).

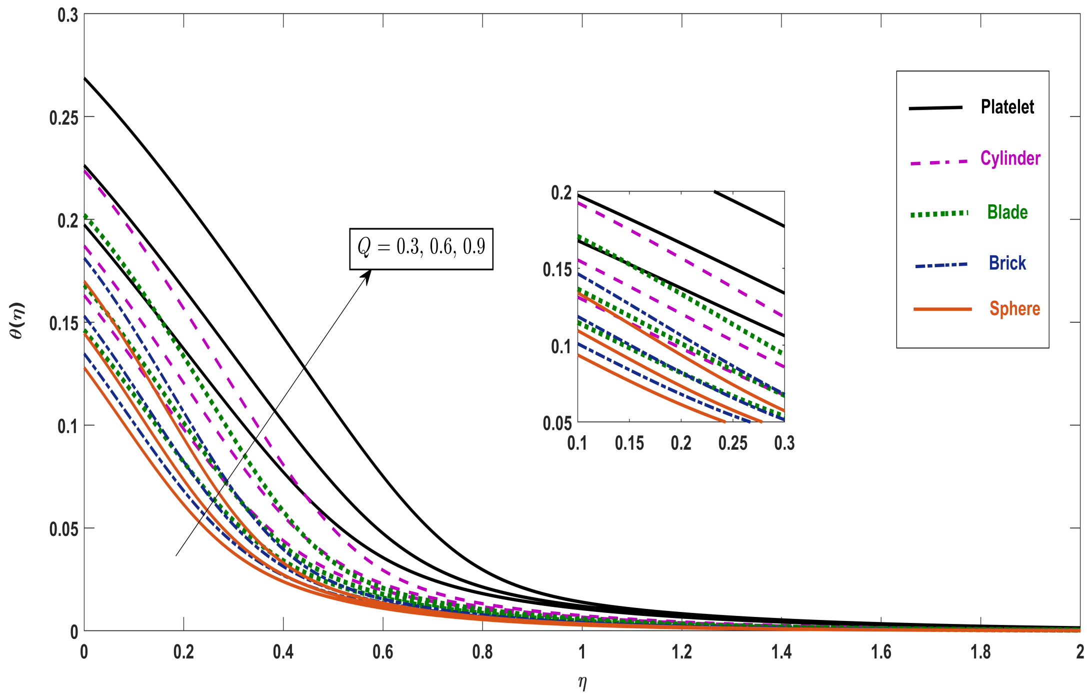

Figure 15. Influence on temperature with external heat generation parameter(Q).

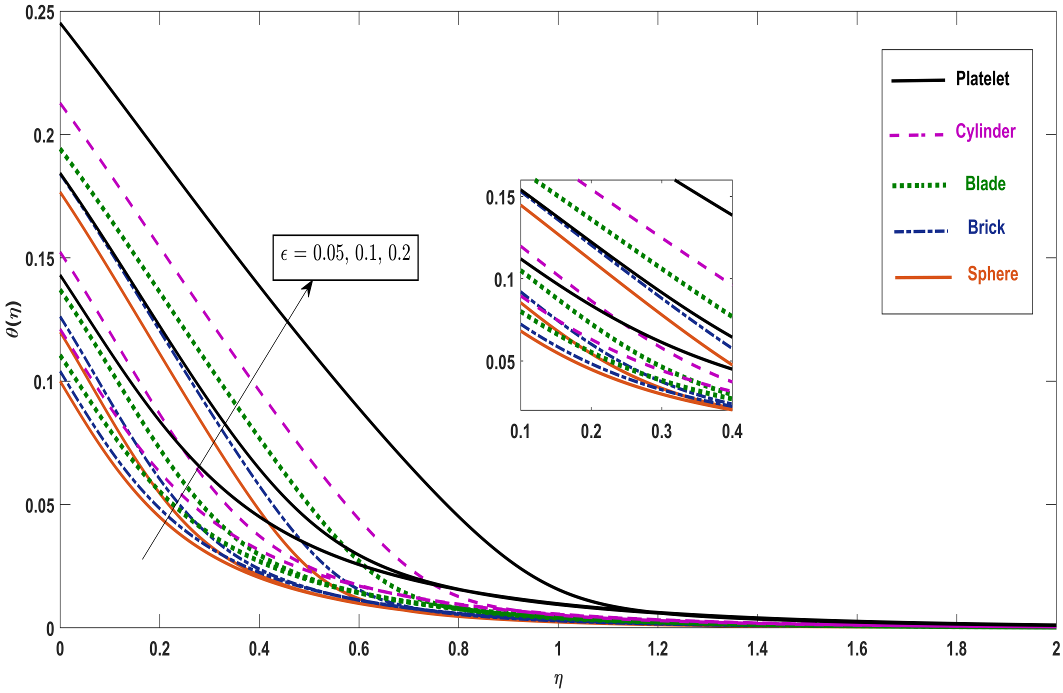

Figure 16. Influence on temperature with thermal conductivity parameter(ϵ).

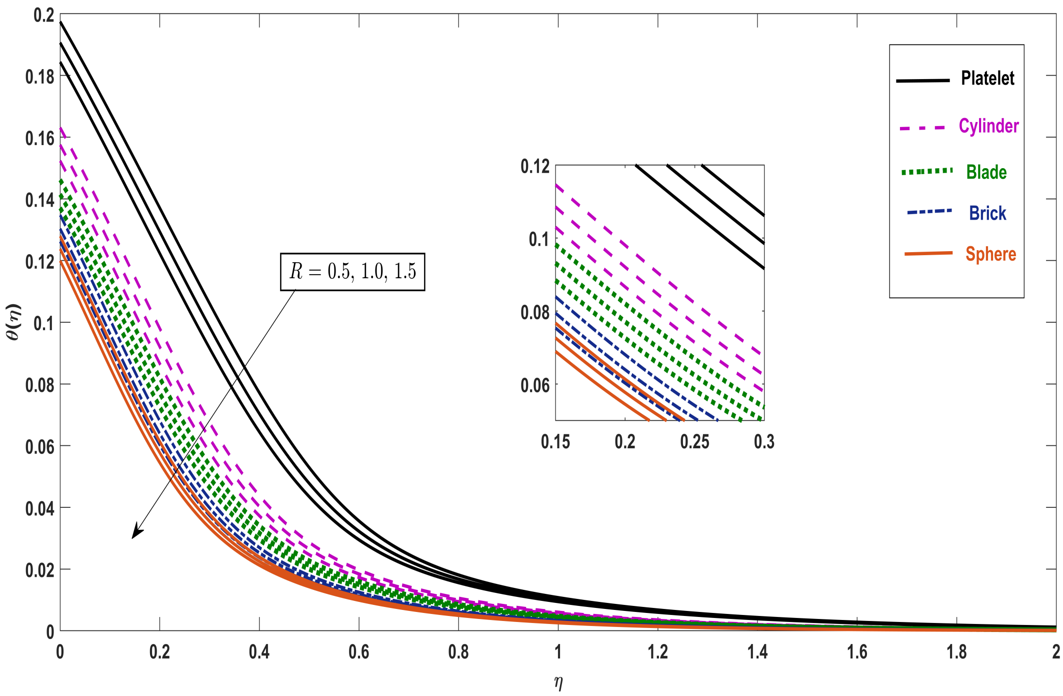

Figure 17. Influence on temperature with viscosity parameter(R).

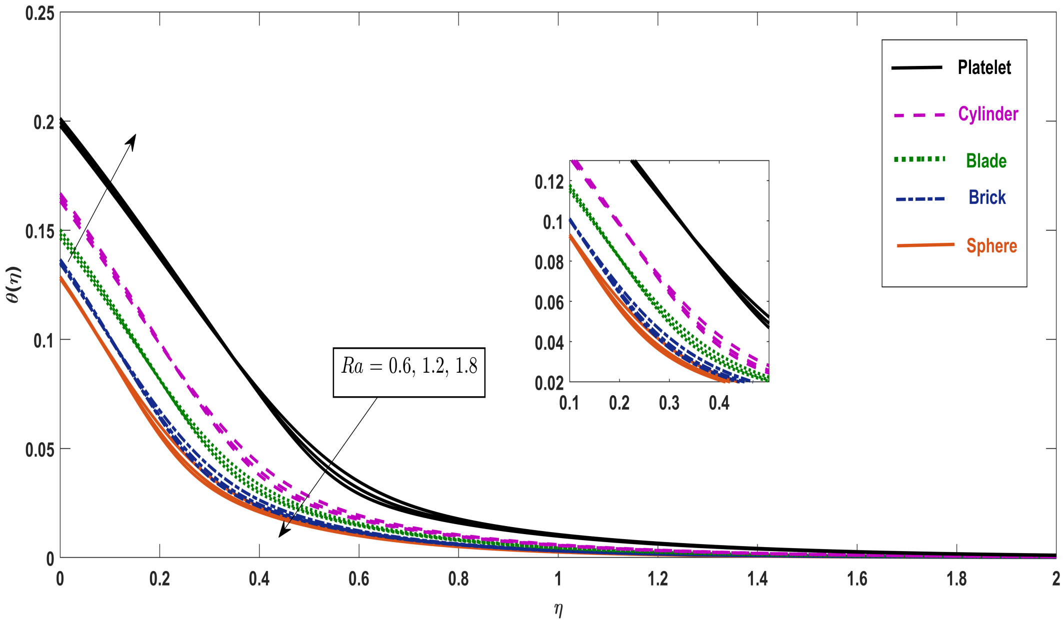

Figure 18. Influence on temperature with radiation parameter(Ra).

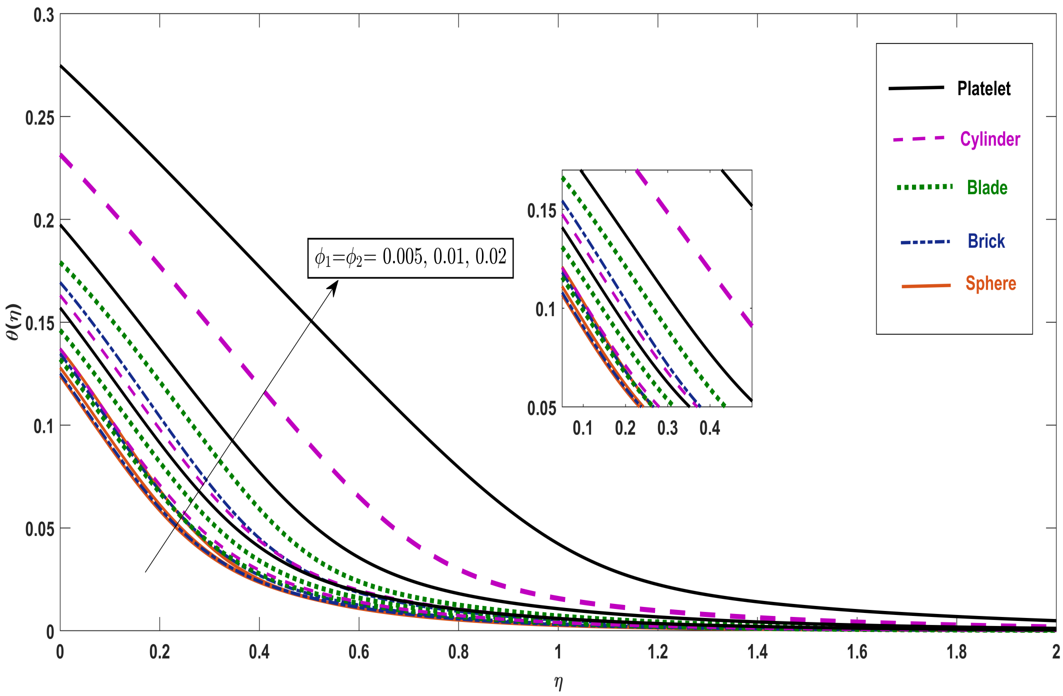

Figure 19. Influence on temperature with volume fraction of nanoparticles(ϕ_1 and ϕ_2).

Table 3. Values of skin friction coefficient.

Parameters										$-C_f Re^{\frac{1}{2}}$				
M	J	N_s	F_w	Bi	E_k	Q	R	ϵ	ϕ_1=ϕ_2	Platelet	Cylinder	Blade	Brick	Sphere
0.4	0.4	0.3	0.3	0.4	0.2	0.3	0.5	0.1	0.01	1.69	1.41	1.32	1.20	1.14
0.3										1.67	1.39	1.31	1.18	1.13
0.6										1.73	1.44	1.35	1.22	1.17
0.9										1.79	1.49	1.39	1.26	1.20
	0.4									1.69	1.41	1.32	1.20	1.14
	0.8									1.78	1.48	1.38	1.25	1.19
	1.2									1.86	1.54	1.44	1.29	1.23
		0.3								1.69	1.41	1.32	1.20	1.14
		0.6								1.31	1.06	0.99	0.88	0.83
		0.9								1.07	0.86	0.79	0.70	0.66
			0.3							1.69	1.41	1.32	1.20	1.14
			0.6							1.93	1.63	1.53	1.39	1.33
			0.9							2.16	1.84	1.73	1.58	1.51
				0.1						1.72	1.43	1.33	1.21	1.15
				0.4						1.69	1.41	1.32	1.20	1.14
				0.7						1.66	1.38	1.30	1.18	1.12
					0.1					1.72	1.43	1.34	1.21	1.16
					0.3					1.66	1.38	1.30	1.18	1.12
					0.5					1.60	1.33	1.25	1.13	1.08
						0.3				1.69	1.41	1.32	1.20	1.14
						0.6				1.68	1.40	1.31	1.19	1.14
						0.9				1.66	1.39	1.30	1.18	1.13
							0.5			1.69	1.41	1.32	1.20	1.14
							1.0			1.62	1.36	1.28	1.16	1.11
							1.5			1.56	1.31	1.24	1.12	1.08
								0.05		1.61	1.34	1.26	1.14	1.09
								0.1		1.56	1.31	1.24	1.12	1.08
								0.2		1.48	1.25	1.18	1.07	1.03
									0.005	1.34	1.20	1.18	1.11	1.10
									0.01	1.69	1.41	1.32	1.20	1.14
									0.02	2.60	2.06	1.64	1.48	1.23

Table 4. Values of Nusselt number.

Parameters												$NuRe^{-\frac{1}{2}}$				
M	J	N_s	F_w	Bi	E_k	Q	R	ϵ	$\phi_1{=}\phi_2$	Ra	Pr_v	Platelet	Cylinder	Blade	Brick	Sphere
0.4	0.4	0.3	0.3	0.4	0.2	0.3	0.5	0.1	0.01	0.5	13	0.51	0.49	0.48	0.47	0.46
0.3												0.52	0.50	0.49	0.48	0.47
0.6												0.50	0.48	0.47	0.46	0.45
0.9												0.49	0.47	0.46	0.45	0.44
	0.4											0.51	0.49	0.48	0.47	0.46
	0.8											0.53	0.51	0.50	0.49	0.48
	1.2											0.54	0.52	0.51	0.50	0.49
		0.3										0.51	0.49	0.48	0.47	0.46
		0.6										0.53	0.51	0.50	0.49	0.48
		0.9										0.54	0.52	0.51	0.50	0.49
			0.3									0.51	0.49	0.48	0.47	0.46
			0.6									0.55	0.53	0.52	0.51	0.50
			0.9									0.57	0.55	0.54	0.53	0.52
				0.1								0.18	0.17	0.16	0.15	0.14
				0.4								0.51	0.49	0.48	0.47	0.46
				0.7								0.83	0.80	0.78	0.76	0.74
					0.1							0.55	0.53	0.52	0.51	0.50
					0.3							0.48	0.46	0.45	0.44	0.43
					0.5							0.40	0.38	0.37	0.36	0.35
						0.3						0.51	0.49	0.48	0.47	0.46
						0.6						0.49	0.47	0.46	0.45	0.44
						0.9						0.47	0.45	0.44	0.43	0.42
							0.5					0.51	0.49	0.48	0.47	0.46
							1.0					0.52	0.50	0.49	0.48	0.47
							1.5					0.52	0.50	0.49	0.48	0.47
								0.05				0.53	0.51	0.50	0.49	0.48
								0.1				0.51	0.49	0.48	0.47	0.46
								0.2				0.48	0.46	0.45	0.44	0.43
									0.005			0.52	0.50	0.49	0.48	0.47
									0.01			0.51	0.49	0.48	0.47	0.46
									0.02			0.50	0.48	0.47	0.46	0.45
										0.6		0.54	0.52	0.51	0.50	0.49
										1.2		0.74	0.71	0.69	0.67	0.65
										1.8		0.93	0.90	0.88	0.86	0.84
											10	0.52	0.50	0.49	0.48	0.47
											13	0.51	0.49	0.48	0.47	0.46
											16	0.50	0.48	0.47	0.46	0.45

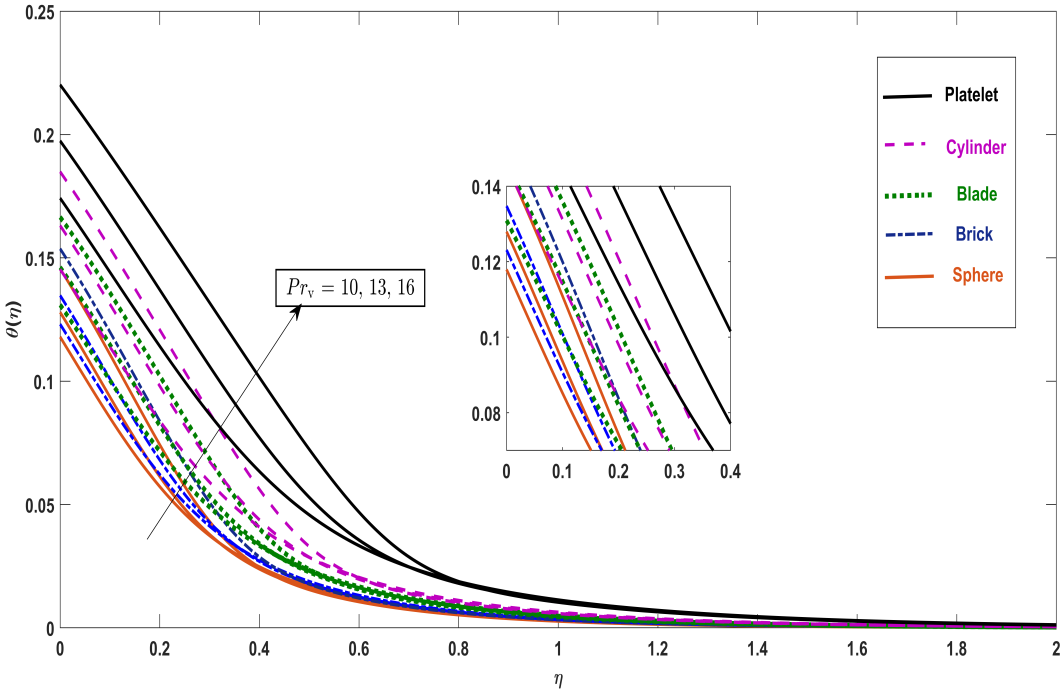

Figure 20. Influence on temperature with prandtl number(Pr_{v}).

Table 5. Comparison of $f''(0)$ for different values of N_s.

N_s	Kumar et al. [25]	Hayat et al. [24]	Ragavi et al. [18]	Present
0	1.186223624	1.1737	1.186223624	1.19058695879
0.01	1.170260409	1.1534	1.153485	1.16985778264
0.05	1.110864508	1.0799	1.079964	1.09469597800
0.1	1.045265031	1.0018	1.001850	1.015000106377
0.5	0.717866798	0.6505	0.650555	0.659025106695
1	0.521172111	0.4625	0.462547	0.46917499065
2	0.339439680	0.2990	0.290990	0.303912713790

Table 6. Validation of stability and accuracy of the solutions by BVP4C.

RelTol	Mesh point	$f''(0)$	$\theta'(0)$	Remark
10^{-3}	10	-0.013257873	0.317892219	Less accurate
10^{-5}	50	-0.013257682	0.317892546	Improving
10^{-7}	100	-0.013257682	0.317892550	Stable
10^{-10}	200	-0.013257682	0.317892550	Converged

which we use in numerical computations were selected on the basis of previous published work and ensuring practical significance of this study. These physical parameters are employed in the range $0.3 \leq N_s \leq 0.9$, $0.3 \leq F_w \leq 0.9$, $0.3 \leq M \leq 0.9$, $0.05 \leq \epsilon \leq 0.2$, $0.5 \leq R \leq 1.5$, $0.1 \leq Bi \leq 0.7$, $0.1 \leq E_k \leq 0.5$, $0.3 \leq Q \leq 0.9$, $0.6 \leq Ra \leq 1.8$, $0.005 \leq \phi \leq 0.2$.

Thermophysical values of hybrid nanoparticles and base fluid are reflected by Table 1. The viscosity coefficient of hybrid nanoparticles for various shape and size are shown in Table 2. The impact of various shape of hybrid nanoparticles on velocity profile are shown in Figure 2, when all other physical parameters N_s=0.3, Bi=0.4, F_w=0.3, J=0.4, Ra=0.5, M=0.4, R=0.5, ϵ=0.1, Q=0.3, E_k=0.2, Pr_{v}=13, ϕ_1=ϕ_2=0.01 are fixed. The velocity profile for hybrid nanoparticles in base fluid PAO oil exhibit an descending order for all shapes of nanoparticles, and descending in the order of platelet, cylinder, blade, brick, and sphere shape, respectively. It shows that platelet shaped nanoparticles have higher velocity compared to all other shapes nanoparticles due to their large surface area which improve momentum exchange with the surrounding fluid layers.

Figure 3 demonstrates that velocity profile decreased for all shapes of nanoparticles with increment into slip parameter(N_s). This is because, the stretching sheet dragging the fluid partially and the velocity of fluid near a sheet is no more equal to the velocity of stretching sheet. The velocity decreased with raising into suction parameter(F_w) as shown by Figure 4. Suction pull out low temperature and low momentum fluid from near wall surface, it suppresses thermal diffusion, and the thermal boundary layer thickness of hybrid nanofluid drop down, hence it decrease the fluid velocity. Figure 5 illustrates the influence in velocity affect by magnetic parameter(M). The consequence shows that the velocity decrease for all shapes nanoparticles, when varying magnetic parameter from 0.3 to 0.9. The acceleration in magnetic field leads to increment into Lorentz force, which is just opposite to fluid flow and this force produce more resistance and degrade velocity of hybrid nanofluid. Figure 6 demonstrates that velocity profile decreased for all shapes of nanoparticles with increment in thermal conductivity parameter(ϵ). This is because, an increment in ϵ causes more attraction between hybrid nanoparticles and it reduces the thermal boundary layer thickness near the sheet. The impact of viscosity parameter(R) on velocity is illustrates by Figure 7. An increment in viscosity of hybrid nanofluid resist the fluid flow due to internal friction and it causes the decrement in velocity profiles for all shapes of nanoparticles. Figure 8 describes the influence in velocity affect by solid volume fraction of nanoparticles. The increment into volume fraction change into the viscosity of hybrid nanoparticles. For sphere shape nanoparticles, it packed effectively in each other and create uniform isotropic drag which increase viscosity and decrease velocity. For other shapes nanoparticles they have anisotropic geometry, which decreased viscosity of hybrid nanofluid and increase the velocity of fluid.

Figure 9 illustrates the influence of temperature profile for all shapes of hybrid nanoparticles, while all other physical parameter are fixed. This shows that platelet shape nanoparticles exhibit high temperature because of larger surface area and the descending order of temperature for all shapes of nanoparticles are platelet, cylinder, blade, brick, and sphere, respectively. Figure 10 describes about the influence in temperature profile affect by slip parameter(N_s). The consequence shows that temperature profile decrease with acceleration in N_s, because it reduce the thickness of thermal boundary layer. Figure 11 demonstrates the influence in temperature profile affect by suction parameter(F_w). It shows that when we accelerate in F_w, then it decreases temperature profile for all shapes of nanoparticles, because it reduces the boundary layer thickness. Figure 12 describes about the influence in temperature profile affect by biot number(Bi). The acceleration in biot number causes more convection and it raising the wall and surface temperature for all shapes nanoparticles.

Figure 13 illustrates the impact of temperature profile on magnetic parameter(M). The temperature profile accelerate with raising in magnetic field for all shapes of nanoparticles because of Lorentz force. Figure 14 shows the influence in temperature profile affect by viscous dissipation(E_k). The fluid temperature enhanced with raising in eckert number because raising into viscous dissipation shows increment in kinetic energy of hybrid nanofluid, which converted into thermal energy and improves temperature distribution. Figure 15 demonstrates the influence in temperature profile affect by internal heat generation parameter(Q). It shows that, acceleration in Q increased the temperature profile for all shapes of nanoparticles. The reason is that increased value of Q indicate temperature storage into the fluid.

The temperature is increased, when we accelerate in thermal conductivity parameter(ϵ) as shown by Figure 16. This happened because it enhance the heat transfer rate from stretching sheet to hybrid nanofluid. The impact of viscosity parameter(R) on temperature is illustrates by Figure 17. The increase value of viscosity parameter increase into the internal friction, which slow down the fluid flow and nanoparticles interact for long time and it reduce the temperature of hybrid nanofluid. Figure 18 describes about the influence in temperature profile affect by radiation parameter(Ra). It illustrates that, temperature profile accelerate on stretching sheet and decrease away from sheet, when we increase radiation parameter. It is because radiation causes heat loss from the stretching sheet, which degrade the temperature profile and convective heat transfer. Figure 19 demonstrates that temperature profile increase with the value of volume fraction(ϕ_1,ϕ_2) increases. The increase value of volume fraction increases thermal conductivity which increase the thermal boundary layer hence it increase the temperature distribution. Figure 20 illustrates the influence in temperature profile affect by variable prandtl number(Pr_{v}). The consequence shows that temperature profile accelerate for all shapes of nanoparticles with raising into Pr_{v}. It reduce the thermal diffusivity in hybrid nanofluid, which increase the thermal boundary layer thickness.

Table 3 demonstrates the influence of various parameters, namely slip parameter (N_s), magnetic parameter (M), suction parameter (F_w), unsteadiness parameter (J), Biot number (Bi), Eckert number (E_k), heat generation parameter (Q), viscosity parameter (R), thermal conductivity parameter (ϵ), and solid volume fraction (ϕ_1, ϕ_2) on the skin friction coefficient for different shapes of (Ag-TiO_2) hybrid nanoparticles. The results show that an increment in parameters M, J, F_w, ϕ_1, and ϕ_2 enhances the magnitude of the skin friction factor $|-C_f Re^{1/2}|$, while an increase in parameters N_s, Bi, E_k, Q, R, and ϵ leads to a reduction in the skin friction factor. Moreover maximum value of skin friction factor noted for platelet shape nanoparticles because it has large flat faces, which increase the resistance to fluid flow near the wall and increase the wall shear stress, While sphere shape nanoparticles has low skin friction because of their isotropic structure which reduce the drag forces and decrease the wall shear stress. The skin friction coefficient decreased in the order of platelet, cylinder, blade, brick, and sphere, respectively.

Table 4 signifies the impact of various parameters such as slip parameter(N_s), magnetic parameter(M), suction parameter(F_w), unsteadiness parameter(J), biot number(Bi), viscosity parameter(R), eckert number(E_k), heat generation parameter(Q), thermal conductivity parameter(ϵ), solid volume fraction(ϕ_1,ϕ_2), radiation parameter(Ra) and prandtl number(Pr_{v}) on nusselt number for various shapes of hybrid nanoparticles over a stretching sheet. It is noticed that nusselt number enhance with increment into parameters J, N_s, F_w, Bi, R, Ra, and opposite trend seen for rising the value of M, E_k, Q, ϵ, ϕ_1,ϕ_2, Pr_{v}. The heat transfer rate is higher for platelet-shaped nanoparticles owing to their greater specific surface area and effective thermal conductivity, which promote enhanced energy exchange with the surrounding fluid. In contrast, sphere-shaped nanoparticles exhibit the lowest heat transfer rate due to their compact isotropic structure and comparatively lower surface-to-volume ratio. The Nusselt number decreases in the order: platelet $>$ cylinder $>$ blade $>$ brick $>$ sphere, which is consistent with the heat transfer enhancement attributed to increasing geometric anisotropy of nanoparticle shape. As evidenced by the data in Table 4 at the baseline parameter set (M=0.4, J=0.4, N_s=0.3, F_w=0.3, Bi=0.4, E_k=0.2, Q=0.3, R=0.5, ϵ=0.1, ϕ_1=ϕ_2=0.01, Ra=0.5, Pr_v=13), the Nusselt number of platelet-shaped nanoparticles surpasses that of cylinder-, blade-, brick-, and sphere-shaped nanoparticles by approximately 4.90%, 5.16%, 9.22%, and 10.57%, respectively.

Table 5 represents the compare between current finding to earlier finding for different values of N_s, the current finding strongly agrees with previous results. The stability and accuracy of BVP4C code verified by varying the relative tolerance(Rel Tol) shown by Table 6. It shows computed physical quantities converges(Rel Tol 10^{-10} considered in our code) with decreasing tolerance which confirming the stability and mesh independence of the solutions.

5 Conclusions

The work illustrates about shape effect of ($Ag-TiO_2$) hybrid nanoparticles along a unsteady radially stretching sheet with suction, slip and thermal radiation effects taking variable thermal conductivity and viscosity. The transform non linear differential equations are solved by numerically technique BVP4C. The effects of several physical parameter on velocity and temperature profile are discuss through graphs and tables. In this research many shapes such as platelet, cylinder, blade, brick, and sphere are consider.

The results are as follow

- The velocity and temperature profile are decreases with raising into slip, suction, and viscosity parameters.
- The velocity profile decreases with raising into magnetic parameter and thermal conductivity parameter.
- An increment into volume fraction of hybrid nanoparticles, the velocity profile decrease for sphere shape nanoparticles and increase for all other shapes nanoparticles.
- The temperature profile increases with rising magnetic parameter, Eckert number, Biot number, heat generation parameter, thermal conductivity parameter, variable Prandtl number, and solid volume fraction of the hybrid nanoparticles. In contrast, an increase in the viscosity parameter (R) leads to a reduction in the temperature profile due to the augmented internal friction that retards the fluid motion and reduces energy dissipation into the thermal boundary layer.
- An increment into radiation parameter, temperature profile increase on stretching sheet and decrease away from stretching sheet.
- The consequences show that platelet shape nanoparticles has high velocity and higher heat transfer rate and descending order of velocity and heat transfer rate are platelet, cylinder, blade, brick, and sphere shape, respectively.
- The heat transfer enhancement of platelet-shaped nanoparticles over cylinder, blade, brick, and sphere shapes ranges from approximately 4.90% to 10.57%, confirming that geometric anisotropy of nanoparticle shape plays a critical role in thermal performance. Furthermore, increasing the radiation parameter (Ra) and viscosity parameter (R) both contribute to an improvement in the heat transfer rate.
- Platelet shape nanoparticles has higher wall shear force in magnitude compare to all other shapes.

This present work can be further extended for three dimensional MHD flow of different types of fluids such as casson fluid, ternary hybrid nanofluid and non newtonian viscous fluid taking variable viscosity, thermal conductivity and electrical conductivity. Other surface geometry can be taken like cylindrical surface, double rotating disk, vertical plate etc. Also, this study can be done by ANN(Artificial neural network) technique in Machine Learning with different assumptions.

Data Availability Statement

Data will be made available on request.

Funding

This work was supported without any funding.

Conflicts of Interest

The authors declare no conflicts of interest.

AI Use Statement

The authors declare that no generative AI was used in the preparation of this manuscript.

Ethical Approval and Consent to Participate

Not applicable.

References

[1] Choi, S. U. (1995, November). Enhancing thermal conductivity of fluids with nanoparticles. In *ASME international mechanical engineering congress and exposition* (Vol. 17421, pp. 99-105). American Society of Mechanical Engineers. [CrossRef]

[2] Saeed, A., Jawad, M., Alghamdi, W., Nasir, S., Gul, T., & Kumam, P. (2021). Hybrid nanofluid flow through a spinning Darcy–Forchheimer porous space with thermal radiation. *Scientific reports, 11*(1), 16708. [CrossRef]

[3] Zeeshan, Khan, I., Weera, W., & Mohamed, A. (2022). Heat transfer analysis of Cu and Al2O3 dispersed in ethylene glycol as a base fluid over a stretchable permeable sheet of MHD thin-film flow. *Scientific Reports, 12*(1), 8878. [CrossRef]

[4] Gupta, R., Gaur, M., Al-Mdallal, Q., Purohit, S. D., & Suthar, D. L. (2022). Numerical study of the flow of two radiative nanofluids with Marangoni convection embedded in porous medium. *Journal of Nanomaterials, 2022*(1), 7880488. [CrossRef]

[5] Dadheech, P. K., Agrawal, P., Sharma, A., Dadheech, A., Al-Mdallal, Q., & Purohit, S. D. (2021). Entropy analysis for radiative inclined MHD slip flow with heat source in porous medium for two different fluids. *Case Studies in Thermal Engineering, 28*, 101491. [CrossRef]

[6] Turkyilmazoglu, M., & Alotaibi, A. (2025). MHD front and rear stagnation-point flow of a moving permeable flat surface. *Physica D: Nonlinear Phenomena*, 135075. [CrossRef]

[7] Iqbal, A., & Abbas, T. (2023). A study on heat transfer enhancement of copper (Cu)-ethylene glycol based nanoparticle on radial stretching sheet. *Alexandria Engineering Journal*, *71*, 13-20. [CrossRef]

[8] Jangid, S., Mehta, R., Bhatnagar, A., Alotaibi, M. F., & Ahmad, H. (2024). Heat and mass transfer of hydromagnetic williamson nanofluid flow study over an exponentially stretched surface with suction/injection, buoyancy, radiation and chemical reaction impacts. *Case Studies in Thermal Engineering*, *59*, 104278. [CrossRef]

[9] Shahzad, A., Ali, R., Hussain, M., & Kamran, M. (2017). Unsteady axisymmetric flow and heat transfer over time-dependent radially stretching sheet. *Alexandria Engineering Journal*, *56*(1), 35-41. [CrossRef]

[10] Kumar, C., & Madasu, K. P. (2026). Impact of magnetic field and permeability on the unsteady slow rotation of a sphere: slip condition. *Archive of Mechanical Engineering*. [CrossRef]

[11] Turkyilmazoglu, M. (2024). Two models on the unsteady heat and fluid flow induced by stretching or shrinking sheets and novel time-dependent solutions. *ASME Journal of Heat and Mass Transfer*, *146*(10), 101802. [CrossRef]

[12] Ali, R., Iqbal, A., Abbass, T., Arshad, T., & Shahzad, A. (2024). Unsteady flow of silica nanofluid over a stretching cylinder with effects of different shapes of nanoparticles and Joule heating. *Archives of Thermodynamics*, *45*(3). [CrossRef]

[13] Rafique, K., Mahmood, Z., & Khan, U. (2023). Mathematical analysis of MHD hybrid nanofluid flow with variable viscosity and slip conditions over a stretching surface. *Materials Today Communications*, *36*, 106692. [CrossRef]

[14] Yahaya, R. I., Arifin, N. M., Ali, F. M., & Isa, S. S. P. M. (2022). Nanoparticle shapes effects on MHD flow of hybrid nanofluid over a stretching/shrinking sheet with slip and chemical reaction. *Journal of Nano Research*, *75*, 139-158. [CrossRef]

[15] Patel, H. R., Mittal, A. S., & Darji, R. R. (2019). MHD flow of micropolar nanofluid over a stretching/shrinking sheet considering radiation. *International Communications in Heat and Mass Transfer*, *108*, 104322. [CrossRef]

[16] Yusuf, A., Bhatti, M. M., & Ellahi, R. (2025). Thermal and sensitivity analysis on regularized curved solar panels using non-Newtonian quaternary hybrid nanofluids: Applications in solar collectors. *Journal of the Indian Chemical Society*, 102256. [CrossRef]

[17] Kumar, C., & Madasu, K. P. (2025). Time-dependent rotational motion of a solid sphere in a Jeffrey fluid with velocity slip. *Physics of Fluids*, *37*(8). [CrossRef]

[18] Ragavi, M., & Poornima, T. (2024). Enhanced heat transfer analysis on Ag-Al 2 O 3/water hybrid magneto-convective nanoflow. *Discover Nano*, *19*(1), 31. [CrossRef]

[19] Yusuf, A., Bhatti, M. M., & Ellahi, R. (2025). Study of ionic water/graphene nanofluids in solar panels under the effects of thermal radiation and slip conditions using experimental data. *International Communications in Heat and Mass Transfer*, *164*, 108845. [CrossRef]

[20] Yang, H., Hayat, U., Shaiq, S., Shahzad, A., Abbas, T., Naeem, M., ... & Zahid, M. A. (2023). Thermal inspection for viscous dissipation slip flow of hybrid nanofluid (TiO2–Al2O3/C2H6O2) using cylinder, platelet and blade shape features. *Scientific Reports*, *13*(1), 8316. [CrossRef]

[21] Mahmood, Z., Rafique, K., Ansari, M. A., Ahmed, N., Khan, U., Kumar, A., ... & Shaaban, A. A. (2025). Deep learning investigation of water-based tetra hybrid nanofluid across a shrinking cylinder for variable electrical conductivity with thermal radiation. *Journal of Radiation Research and Applied Sciences*, *18*(1), 101213. [CrossRef]

[22] Yusuf, A., Khan, S. U., Hassan, M., Bhatti, M. M., & Öztop, H. F. (2025). Heat transfer optimization of MWCNT-Al2O3 hybrid nanofluids under convective and irreversible effects. *Journal of Umm Al-Qura University for Applied Sciences*, 1-15. [CrossRef]

[23] Famakinwa, O. A., Koriko, O. K., & Adegbie, K. S. (2022). Effects of viscous dissipation and thermal radiation on time dependent incompressible squeezing flow of CuO-Al2O3/water hybrid nanofluid between two parallel plates with variable viscosity. *Journal of Computational Mathematics and Data Science*, *5*, 100062. [CrossRef]

[24] Hayat, U., Shaiq, S., Shahzad, A., Khan, R., Kamran, M., & Shah, N. A. (2023). The effect of particle shape on flow and heat transfer of Ag-nanofluid along stretching surface. *Chinese Journal of Physics*, *85*, 708-721. [CrossRef]

[25] Kumar, B., & Gupta, R. (2026). Numerical investigation of hybrid nanofluid (TiO 2-Al 2 O 3/water) through nonlinear partial differential equations. *International Journal of Mathematics for Industry*, 2640002. [CrossRef]

[26] Makinde, O. D., & Makinde, A. E. (2023). Thermal analysis of a reactive variable viscosity TiO2-PAO nanolubricant in a microchannel poiseuille flow. *Micromachines*, *14*(6), 1164. [CrossRef]

[27] Ferdows, M., Jahan, S., Tzirtzilakis, E., & Sun, S. (2023). Magnetohydrodynamic hybrid nanofluid flow through moving thin needle considering variable viscosity and thermal conductivity. *Advances in Mechanical Engineering*, *15*(11), 16878132231208272. [CrossRef]

[28] Manigandan, A., & Narayana, P. V. S. (2024). Impact of variable fluid characteristics on MHD hybrid nanofluid (MgO+ ZnO/H2O) flow over an exponentially elongated sheet with non-uniform heat generation. *Case Studies in Thermal Engineering*, *55*, 104077. [CrossRef]